Modeling of Erosion Wear of Sand Water Slurry Flow through Pipe Bend using CFD

V. Singh[1†], S. Kumar[2] and S. K. Mohapatra[1]

[1] Thapar Institute of Engineering and Technology, Patiala, Punjab, 147004, India
[2] National Institute of technology, Jamshedpur, India

†*Corresponding Author Email: varinder8382@gmail.com*

ABSTRACT

In the present study, erosion wear of a 90º pipe bend has been investigated using the Computational fluid dynamics code FLUENT. Solid particles were tracked to evaluate the erosion rate along with k-ε turbulent model for continuous/fluid phase flow field. Spherical shaped sand particles of size 183 μm and 277 μm of density 2631 kg/m³ are injected from the inlet surface at velocity ranging from 0.5 to 8 ms⁻¹ at two different concentrations. By considering the interaction between solid-liquid, effect of velocity, particle size and concentration were studied. Erosion wear was increased exponential with velocity, particles size and concentrations. Predicted results with CFD have revealed well in agreement with experimental results. The magnitude and location of maximum erosion wear were more severe in bend rather than the straight pipe.

NOMENCLATURE

C	drag cofficient		velocity after impact
E_r	erosion rate	V_{pt1}	tangential components of the particle
F_B	bouyancy force		velocity before impact
F_D	drag force	V_{pn2}	tangential components of the particle
F_P	pressure gradient force		velocity after impact
$g_{o,pp}$	distribution function	V_f	volume of fluid
K_{fp}	fluid-Solid particles exchange coefficient	V_p	volume of solid particles
		λ_p	bulk viscosity of solid
K_{pf}	solid particles- fluid exchange coefficient	f	continous fluid
		ρ_f	density of Fluid phase
m_p	solid particle mass flow rate in kg/sec	ρ_m	density of pipe bend material
m_{pf}	mass transformation from phase p to f	ρ_p	density of solid particles
Re	Relative Reynolds number	μ_p	shear viscosity of solid particles
r/D	radius of curvature -to-diameter ratio	$\mu_{p,bul}$	particles bulk viscosity
$\vec{U}_f$	mean phase of flow velocity	v_f	fluid velocity
U_{pn1}	normal components of the particle velocity before impact	$\mu_{p.col}$	particles Collision viscosity
U_{pn2}	normal components of the particle	v_p	solid particles velocity

$\mu_{p,fr}$	particles frictional viscosity	$\bar{\bar{\tau}}_p$	solid particle phase stress tensor
$\mu_{p,kin}$	particles kinetic viscosity	$f(\theta)$	impact angle function
$\bar{\bar{\tau}}_f$	fluid phase stress tensor	θ	Particle impact angle

1. INTRODUCTION

Erosion is the phenomena in which material is removed from the target surface/wall due to continuous impingement of solid particles on it and finally component/part fails with elapse of time. Such erosion problems are found in pipelines, bends, elbows, tees, valves, pumps etc. while transporting liquid-solid, gas-solid mixture through these. In power plants erosion occurs due to the transportation of coal water slurry, ash water slurry (Modi *et al.* 2000) and pneumatic conveying of ash to silo through the pipeline system. Whereas in oil, gas and petroleum production sand particles are entrained which contribute to erosion in the various parts of the pipeline fitting (Edward *et al.*, 2001). Hence erosion phenomenon may be extremely costly; leads to failure of the concerned components or pipeline fittings; require frequent replacement or may arise system's shut down (Edward *et al.* 2001). Sand erosion is also concerned with transportation of sand-water slurry through the pipeline system. Due to a sudden change in the flow direction in bends/elbows, the particles cause much erosion in these sections. (Chen *et al.* 2004, Edward *et al.* 2001, Wang *et al.* 2003).

Many researchers have reported erosion models to evaluate the intensity of erosion of target wall. Some of these models are given by (Finnie *et al.* 1960, Bitter e*t al.* 1963, Neilson and Gilchrist *et al.* 1968, Mclaury *et al.* 2004, Huang *et al.* 2008, Oka *et al.* (2005), Zhang *et al.* 2007) and others through experiments. During the last few years, design and performance analysis of fluid mechanics have experienced great progress with the availability of less expensive high performance computers and user friendly computational fluid dynamics (CFD) software's (J.P. Singh *et al.* 2017, S. Shyji *et al.*, 2017, E. Shirani K. *et al.*, 2011, Talbi *et al.*, 2009, A. Ababaei *et al.*, 2017).

(Zhang *et al.* 2000) have studied the erosion and corrosion in the pipe using glass particles in CFD with the Lagrangian particle track model. (Edward *et al.* 2001) have numerically investigated erosion in standard elbows, long radius elbows and plugged tees. They observed low erosion rate due to efficient momentum transfer from the fluid to particles in long radius bend than plugged tees and standard elbow. They also compared the predicted erosion results with experimental data. Gnanavelu *et al.* (2009), Wang *et al.* 2009, Gnanuvela *et al.* 2011) have also measured erosion on a flat plate through jet impingement test (JIT) and also compared with CFD predicted results as well as with erosion models. (Mazumder *et al.* 2012) have numerically studied the effect of liquid and gas velocities to analyze the maximum erosion magnitude and location in U-bend

with different size of particles. (Okita *et al.* 2012) have studied numerically and experimentally the effect of fluid viscosity on erosion ratio with different size of sand particles at various velocities for water and air flow. (Mansouri *et al.* 2014) have proposed erosion depth equation using CFD predicted data and submerged jet test methodology. (Safaei *et al.* 2014) have presented erosion wear in elbow using water-copper particles flow through CFD. They also studied the effect of solid particles concentration, velocity and particles size. (Shahata *et al.* 2014) has numerically investigated erosion wear in bend using seawater-sand slurry at five different concentrations with laminar and turbulent flow models. (Chen *et al.* 2015) have carried out the simulation to predict the erosion wear in three different pipe bend angles. The maximum erosion was found near the exit of bends and the erosion intensity was decreased for smaller bend angle. (Solnordal *et al.* 2015) have evaluated the erosion by pneumatic conveying of sand particles through a standard elbow.

The results revealed that good agreement with experimental data by considering the wall roughness rather than a smooth wall in the simulation. (Duarte *et al.*, 2017) have numerically and experimentally investigated the low erosion on twisted pipe bend than untwisted. Less erosion was found in elbow due to the swirling of particles in the 4-spiral designed pipe than the 8-spiral designed pipe bend and untwisted pipe bend.

CFD validation had been done with experimental data of (Zeng *et al.* 2014). Hence, CFD is widely used industrial and commercial application to predict the flow behavior of fluid flow and solid particles by imposing the appropriate physical boundary conditions over the CAD-modelled (prototype/model) flow domain. However, for the better understanding of CFD analysis, a physical prototype/model testing may be carried out but it depends upon the industrial application or utility. Wood *et al.* (2004). In the present study, the erosion rate was predicted in horizontal pipe-bend for the flow of sand–water suspension.

2. CFD MODELING

In ANSYS R15.0 software package, a standard 90º H-H pipe bend is made as shown in Fig. 1 and the geometry's detail is given in Table 1. Length of the pipe is sufficient for the fully developed flow through the pipe bend. The properties of carrier fluid and solid particles are described in the Table 2. Hexahedron type elements are used, for CFD post processing simulation. Simulations are carried out at Intel Xenon E51607 v2.30 computer having 2.59

GHz processing unit and 16 GB RAM The governing equations are solved by Navier Stokes equations and the two phase flow Eular- Lagrangian (DPM) is employed in simulation. Eularian model simulates the continuous phase whereas Lagrangian approach tracks the solid particles. k-ε model turbulent model with standard wall function for near wall treatment, SIMPLE algorithm for pressure–velocity coupling and first order upwind schemes are used. Two way-coupling methodology is applied for solid–liquid phases to solve alternatively by considering their effect on each other. Boundary conditions for the flow domain are set to velocity inlet; pressure outlet and wall with no slip condition as well as roughness constant of 0.5 along with convergence residual 10^{-4}. The injected particles ($I = Ni \times Ns$ counted as 12000) from inlet, when impact on the pipe-bend wall reflect back and rebound many times.

Table 1 Geometry description

Diameter, D	r/D ratio	Total length, L	Density, ρ_m	Material
0.1m	1.5	1.5m	7850 kg/m³	Mild Steel
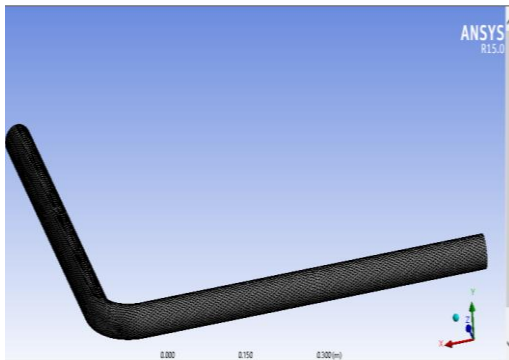
Fig. 1. Meshing of Pipe Bend.

Hence the particles loose their energy in the form of heat dissipation or material deformation of pipe bends (Mansouri *et al.* 2015). This loss of energy of particle is taken into account in the form of coefficient of restitution (COR). COR is the ratio of particle impact velocity to the rebound velocity of particle. The reflection coefficients for solid particles in normal e_n and tangential e_t directions are given below:

$$en = \frac{V_{nt2}}{U_{nt1}} \tag{1}$$

$$et = \frac{V_{pt2}}{U_{pt1}} \tag{2}$$

In this study, the rebound model proposed by (Grant and Tabakoff 1975, 1973) is used. Upn and Vpt are the normal and tangential velocity components of the particle velocity as shown in Fig. 2.

$$e_n = 0.993 - 1.76\theta + 1.46\theta^2 - 0.49\theta^3 \tag{3}$$

$$e_t = 0.998 - 1.66\theta + 2.11\theta^2 - 0.67\theta^3 \tag{4}$$

Where θ is the particle impact angle. The wear mechanism depends upon the normal and tangential impact. So it is assumed that normal impact contributes to deformation and cutting wear is observed with low impact angles up to 18°.
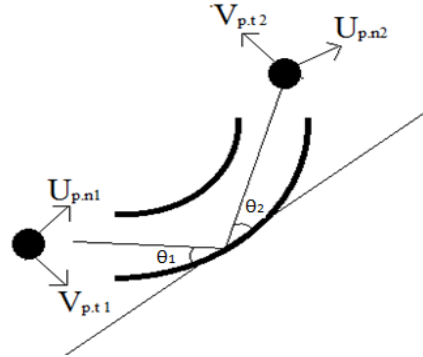
Fig. 2. Impact of particles on curved wall.

2.1 Continuity Equation

The continuity equation is applied to evaluate the volumetric fraction of discrete phase (p) and continuous phase (f), is proposed by (Jashanpreet Singh *et al.* 2018) as given below:

$$\frac{\partial}{\partial t}(a_p \rho_p) + \nabla(a_f \rho_f v_f) = \sum_{p=1}^{n}(m_{pf} - m_{fp}) + S_s \tag{5}$$

In Eq. (5), the mass transformation from phase p to f is denoted by term m_{pf} $\dot{m}_{pf}$ and effective density of discrete phase (p) is denoted by term $\vec{a} = a_p \rho_p$

2.2 Momentum Equations

The momentum equations is proposed (Cheng and Mewes *et al.* 2012) for discrete phase (p) and continuous phase (f) given below:

$$\frac{\partial}{\partial t}(a_f \rho_f \vec{U}_f) + \nabla(a_f \rho_f \vec{U}_f \vec{U}_f) = -a_f \nabla p + \nabla \bar{\bar{\tau}}_f + a_f \rho_f \vec{g} + K_{pf}(\vec{V}_P - \vec{U}_f) \tag{6}$$

$$\frac{\partial}{\partial t}(a_p \rho_p \vec{V}_p) + \nabla(a_p \rho_p \vec{V}_p \vec{V}_p) = -a_p \nabla p - a_f \nabla p_p + \nabla \bar{\bar{\tau}}_p + a_p \rho_p \vec{g} + K_{pf}(\vec{U}_f - \vec{V}_P) \tag{7}$$

Where $\bar{\bar{\tau}}_p$ and $\bar{\bar{\tau}}_f$ $\bar{\bar{\tau}}_f$ are the phase tensor for discretesolid (p) and continouosfluid (f) phases (Cheng and Mewes 2012 and Brennen 2005) are given by:

$$\frac{\partial}{\partial t}(\vec{V}_p) + \nabla(a_p \rho_p \vec{V}_p \vec{V}_p)\bar{\bar{\tau}}_p = a_p \mu_p(\nabla \vec{\vartheta}_p + \nabla \vec{\vartheta}_p^{tr}) + a_p(\lambda_p - \frac{2}{3}\mu_f)\nabla \vec{\vartheta}_p \tag{8}$$

Table 2 Properties of liquid-solid phases

Liquid phase		Solid phase	
Carrier fluid:	Water	Injected particles:	Sand
Density ρ_w:	1000 kg/m^3	Particle density:	2631 kg/m^3
Viscosity μ_w:	0.001003 pa-sec	Particle size:	183 and 277 μm
		Particle shape:	Spherical/Uniform
		Concentration (Cw):	2.5 to 10% (by weight)

$$\bar{\bar{\tau}}_f = a_f\,\mu_f\,(\nabla\vec{\vartheta}_f + \nabla\vec{\vartheta}_f{}^{tr}) \tag{9}$$

In Eq. (6), K_{pf} represents the solid-liquid exchange coefficient wheares $K_{pf} = K_{fp}$.

$$K_{pf} = 150\frac{a_p(1+a_f)\mu_f}{a_f\,d_p^2} + 1.75\frac{\rho_f\,a_p\left|\vec{V}_p - \vec{U}_f\right|}{d_p} \tag{10}$$

In Eq. (7),

$$p_p = (a_p\rho_p\theta_p) + 2\rho_p(1+e_{pp})a_p^2 g_{o.pp}.\theta_p$$

where, $g_{o.pp}$ represents the intermolecular collision between grains of the solid particles, (Cheng and Mewes 2012 and Brennen 2005) represented as:

$$p_p = (a_p\rho_p\theta_p) + 2\rho_p(1+e_{pp})a_p^2 g_{o.pp}.\theta_p$$

$$g_{o,pp}\cdot = \left[1 - \left(\frac{a_p}{a_{p,\max}}\right)^{\frac{1}{3}}\right]^{-1} \tag{11}$$

In Eq. (8), λ_p represents the bulk viscosity between particles of discrete phase (Chen, L. *et al*. 2009) is given by:

$$\lambda_p = \frac{4}{3}(a_p\rho_p d_p g_{o.pp})(1+e_{pp})\left(\frac{\theta_p}{\pi}\right)^{\frac{1}{2}} \tag{12}$$

μ_p Represents the shear viscosity of discrete phase solid particles which rises due to the momentum exchange between solid particles by means of collision and translation (Duan *et al*. 2009) can be written as:

$$\mu_p = \mu_{p,col} + \mu_{p,kin} + \mu_{p,bulk} \tag{13}$$

In above equation, terms $\mu_{p,col}$, $\mu_{p,kin}$ $\mu_p,bulk$ indicates the collisional, kinetic and bulk viscosities which are simplified as:

$$\mu_p,col = \frac{4}{5}(a_p\rho_p d_p g_{o.pp})(1+e_{pp})\left(\frac{\varphi_p}{\pi}\right)^{\frac{1}{2}} \tag{14}$$

$$\mu_p,kin = \left[\frac{10\rho_p d_p\sqrt{\theta_p\pi}}{96a_p(1+e_{pp})g_{o.pp}} + \left[1+\frac{4}{5}a_p\rho_p d_p g_{o.pp})(1+e_{pp})\right]^2 a_p\right] \tag{15}$$

$$\mu_p,bulk = \frac{p_p\sin\phi}{2\sqrt{I_{2p}}} \tag{16}$$

$$\frac{\partial\rho_f\,k}{\partial t} + \nabla.(\rho_f\vec{V}_f\,k) = \nabla\left(\mu+\frac{\mu_t}{\sigma_\in}\right).\nabla k + G_k\rho_f\in \tag{17}$$

$$\frac{\partial\rho_f\in}{\partial t} + \nabla(\rho_f\vec{V}_f\in) = \nabla\left(\mu+\frac{\mu_t}{\sigma_\in}\right).\nabla\in +\frac{\in}{k}\left(C_{\in 1}G_k - \rho\in C_{\in 2}\right) \tag{18}$$

$$U_f = \overline{U_f} + U_f' \tag{19}$$

Where, term $\overline{U_f}$ represnts the mean phase of flow velocity. Equation (19) predicts the value of liquid flow fluctuating velocity in large number of iterations that evaluates the dispersion of solid particles due to the turbulence effect.

2.2 Particle Tracking Equation According to Newton's Second Law

Trajectories of Particle are tracked by the Euler-Lagrange Model in which a number of iteration is apply on equation to find a solution. A number of trajectories of particles are used to make perfect wall collision sites of particle. In the current study, a k- ε turbulence model is using to track the discrete phase in the flow field (Dewan *et al*., 2011):

$$m_p\frac{dV_p}{dt} = F_A + F_B + F_D + F_P \tag{20}$$

Added force:

$$F_A = -\frac{1}{12}\pi d_p^3 \rho_p \frac{dV_p}{dt} \qquad (21)$$

Buoyancy force:

$$F_B = \frac{1}{6}\pi d_p^3 (\rho_p - \rho_f)g \qquad (22)$$

$$F_D = C_D \rho_f \frac{\pi d_p^2}{8}\left|V_f - U_p\right|(U_f - V_p) \qquad (23)$$

C_D is Drag coffiecient given by:

$$C_D = \frac{24}{\text{Re}}\left(1 + 0.15\text{Re}^{0.687}\right) \qquad (24)$$

Re is Relative Reynolds number. The Reynolds number obtain after dividing the inertia to viscous force. It determined the fluctuation of the discrete phase (p) and continuous phase (f). The equation is written as:

$$\text{Re} = \frac{\rho_p d_p \left|V_p - U_f\right|}{\mu_f} \qquad (25)$$

F_P is Pressure Gradient force:

$$F_p = \frac{1}{4}\pi d_p^3 \nabla P \qquad (26)$$

2.3 CFD Based Erosion Wear Model

Discrete phase model (DPM) is applied to predict the erosion wear in the pipe bend for the flow of solid-liquid suspension. DPM solves the generalized erosion wear equation tracks the solid particles in fluid flow. (Edwards 2000)

$$E_r = \frac{\sum_{p=1}^{N_{particle}} m_p P_s f(\theta)V_p^n}{A_{face}} \qquad (27)$$

Where P_s is taken as 1 for triangular, 0.53 for semi-round, 0.2 for spherical shape, n is velocity exponent varies from 2 to 3 for ductile material.

Validation of Numerical Model

Present simulation results are validated with Experimental data of (Zeng *et al* 2014). They experimentally measured the erosion corrosion in 90° elbow having diameter of 50 mm and radius of curvature of 76.9 mm. For fully developed flow, the horizontal and vertical lengths of the pipe were taken as 1m and 0.5 m respectively. They used the spherical shape of sand particles with the size of 450 μm. The flow velocity is taken as 4 ms⁻¹. The parameters used in simulation are mentioned in Table 3. Figure 3 shows the comparison between present simulation results and experimental data of (Zeng *et al*. 2014) at Φ = 180° of pipe bend. Although the predicted CFD simulation results having ±12% error but model shows relatively good in agreement

with (Zeng *et al*. 2014) experimental data.

Table 3 Experimental data of (Zeng *et al*. 2014)

Parameter	Description
Carrier fluid	Water
Carrier fluid density	1000 kg/m³
Solid particles	Sand
Particle diameter	450μm
Solid particles mass flow rate	235g/sec
Pipe material density	7800kg/m³
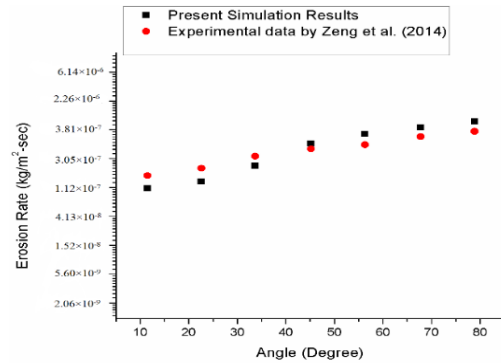
Fig. 3. Comparison of Predicted results with experimental data of (Zeng *et al*. 2014).

3. RESULTS AND DISCUSSION

3.1 Effect of Particle Velocity

In the solid liquid flow of water and sand particles, the sand particles can be assumed to be analogous to the gas particles, and all the laws which control/define their motion can also be used to great extent for the solid particles dispersed in a liquid phase. So according the kinetic theory, the solid particles at higher velocities possess a higher kinetic energy. The randomness in the particle's motion is reported to increase exponentially with kinetic energy. So, in the case of the sand particles, the motion is more random at higher velocities (6-8 ms⁻¹). As a result, greater erosion is expected at 6-8 ms⁻¹. In the present case, the erosion wear of the subjected parts is observed to increase exponentially. As the velocity increases 0.5-2, 2-4, 4-6, 6-8 ms⁻¹ the momentum of the impacting particles also increases, which corresponds to maximum erosion rate at bend section rather than straight pipe. At the low flow velocity most of the particles settle down and slide slowly over the lower side of the pipe-bend where the erosion severity exists as shown in Fig. 4 As velocity gradually increases from 0.5 to 8 ms⁻¹, particles start to entrain into the flowing fluid and due to the momentum, particles deviate from the streamline in curved section and hence strike on Extrados wall of the bend as shown in Fig. 4 where high erosion wear is observed. Hence, the effect of particle velocity is observed as presented in Fig. 5, in which the erosion rate is increasing with particles velocity.
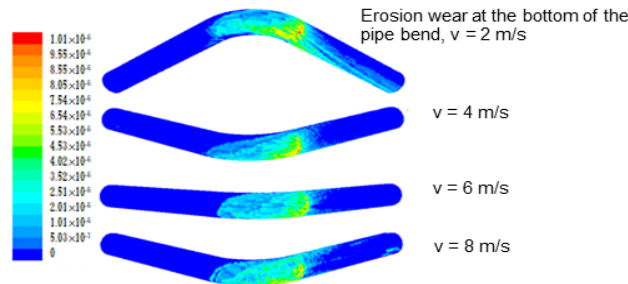
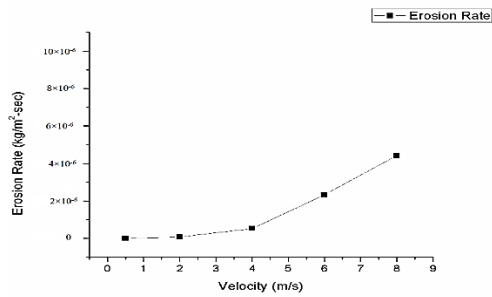**Fig. 4. Locations of erosion wear of bend section at different velocities.**

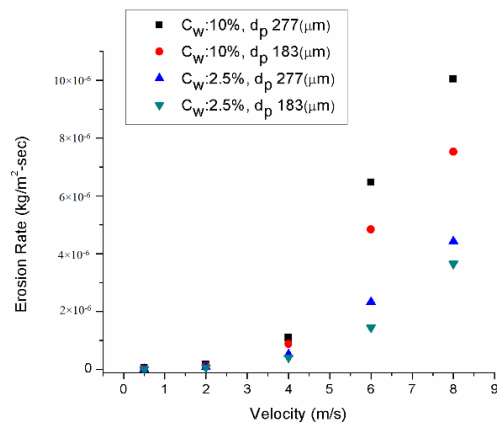**Fig. 5. Effect of velocity on erosion wears of Pipe Bend.**

Fig. 6. Effect of particle concentration and particles size at different velocities.

3.3 Effect of Solid Concentration

Generally, the erosion severity is increased with the solid particles concentration. So, the predicted results are good in agreement with previous experimental and numerical approaches used by many authors. The increase in the concentration does not always increase the erosion percentage correspondingly; sometimes the percentage may decrease due to the deposition or settling of particles at bottom region in the pipe-bend wall. This deposition or settling of particles is because of low flow velocity of particles which tends to decrease in erosion percentage or low erosion wear at bottom side in pipeline. However, increasing the solid phase concentration leads to increase in

pressure drop in pipe line during the slurry transportation.

3.2 Effect of Particle Size

The results shown by Fig. 6 reveal that the lowest erosion wear is predicted for 183μm particle size of sand particles as compared to 277μm sand particle for all velocities and concentrations. Although particles size do not show any significantly results for low velocity up to 2 m/s after that erosion rate is increasing instantly for both concentrations and velocities. For 183μm sand particles size, the maximum erosion wear percentage is increased by 1.36, 2.06, 2.36, 1.06% at velocities ranging from 0.5-2, 2-4, 4-6 and 6-8 ms^{-1} for concentration of 2.5% respectively. Similarly for 277μm, erosion rate is increased by 2.80, 1.09, 2.21, and 1.26% at velocities ranging from 0.5-2, 2-4, 4-6 and 6-8 ms^{-1} respectively.
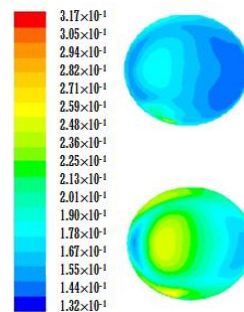

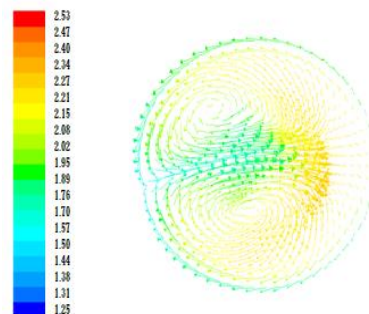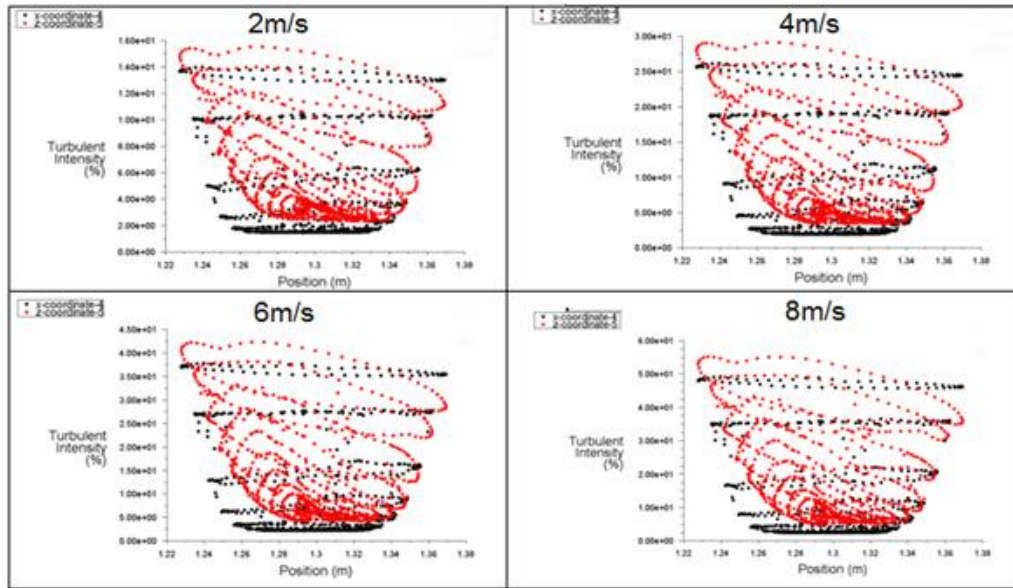**Fig. 7. Intensity of Turbulence inlet and outlet of Pipe Bend.**

Fig. 8. Velocity vector at bend outlet.

Fig. 9. Turbulence intensity distribution on bend inlet (black) and outlet (red) sections.

3.4 Turbulence Intensity Distributions

Figure 7 and Fig. 9 show the turbulence intensity of solid liquid inside the pipe bend before (black) and after (red) the bend section. The turbulence intensity is found to be uniform at the bend inlet section but in the curved section the turbulence intensity is observed to increase at the region close to bend's intrados. This happens due to the centripetal force of action in the curved section. As a result of which particles are seems to be moving from the outer radii to inner radii of pipe-bend section as shown in Fig. 8. Particles start moving from the interior wall and strike the exterior wall, causing erosion at the wall. Figure 9 clearly depicts the aforementioned statement, indicative from the velocity vectors. Therefore, the turbulence intensity is observed to increase from 14 to 15, 25 to 28, 36 to 42, 48 to 57% at velocities of 2, 4, 6, 8 ms^{-1}, respectively.

3.5 Erosion Rate Distributions

Figure 4 shows the erosion rate on the pipe bend wall at different velocity. At velocities of 2 ms^{-1} and 4 ms^{-1} the erosion rate becomes 5×10^{-8} kgm^{-2}s^{-1} at distance of 1.3 m and 4.25×10-8 kgm^{-2}s^{-1} at distance 1.33 m. whereas at higher velocity 4-6 and 6-8 ms^{-1} the erosion rate is observed 4.80×10^{-6} kgm^{-2}s^{-1} and 1×10^{-5} kgm^{-2}s^{-1} at the distance of 1.32 m and 1.37 m respectively.

4. CONCLUSION

In the present study, a CFD based erosion model is employed to evaluate the erosion rate in horizontal pipe bend. Also, the effects of particles velocity, particles size and solid concentration have been studied

- The predicted results show that the erosion rate is influenced by particle impact velocity. An exponential relationship take place between erosion rate and particle impact.

- At low velocity, erosion is observed at the bottom side of the pipe bend due to settling and low inertia as well as gravitational acting force in the particles.

- Maximum erosion rate is predicted in curved section rather than straight one. Maximum erosion magnitude is observed at location of 1.33m (approx.) for different velocities.

- As the velocity is increased, the maximum erosion location is shifted toward the convex side of the bend due to centripetal force of action.

- Solid particles concentration and particle size contribute significantly to increase in erosion rate. As the solid concentration is increased, the probability and frequency of particle-pipe collisions increases. This increase is observed to a certain value of solid concentration. As the concentration is increased beyond this limit, the particles start settling at the bottom of the pipe, which further reduces the collisions between pipe and the particles. The larger particles have greater momentum as compared to the smaller particles. As a result, the larger particles cause greater erosion as compared to the smaller ones

- Due to the momentum in the particles turbulence intensity increase in inner side of the bend rather than outer size.

REFERENCES.

Ababaei, A., A. A. Arani and A. Aghaei (2017). Numerical Investigation of Forced Convection of Nanofluid Flow in Microchannels: Effect of Adding Micromixer. *Journal of Applied Fluid Mechanics* 10(6), 1759-1772.

Bitter, J. G. A. (1963) A study of erosion phenomena: Part I, *Wear*, 6 5 - 21.

Brennen, C. E., and C. E. Brennen (2005). *Fundamentals of multiphase flow*. Cambridge university press.

Chen, J., Y. Wang, X. Li, R. He, S. Han and Y. Chen (2015). Erosion prediction of liquid-particle two-phase flow in pipeline elbows via CFD–DEM coupling method. *Powder Technology* 275, 182-187.

Chen, L., Y. Duan, W. Pu and C. Zhao (2009). CFD simulation of coal-water slurry flowing in horizontal pipelines. *Korean journal of chemical engineering* 26(4), 1144-1154.

Chen, X., B. S. McLaury and S. A. Shirazi (2004). Application and experimental validation of a computational fluid dynamics (CFD)-based erosion prediction model in elbows and plugged tees. *Computers & Fluids* 33(10), 1251-1272.

Cheng, L. Mewes, D. (Eds.). (2012). *Advances in multiphase flow and heat transfer* (Vol. 3). Bentham Science Publishers.

Dewan, A. (2011). Some Case Studies. In *Tackling Turbulent Flows in Engineering* (pp. 105-115). Springer, Berlin, Heidelberg.

Duarte, C. A. R. and F. J. de Souza (2017). Innovative pipe wall design to mitigate elbow erosion: A CFD analysis. *Wear* 380, 176-190.

Duarte, C. R., M. Olazar, V. V. Murata and M. A. S. Barrozo (2009). Numerical simulation and experimental study of fluid–particle flows in a spouted bed. Powder Technology 188(3), 195-205.

Edwards J. K., B. S. McLaury and S. A. Shirazi (2001). Modeling Solid Particle Erosion in Elbows and Plugged Tees. *Journal of Energy Resources Technology*, 123, 277-284.

Edwards, J. K. (2000). *Development, validation, and application of a three-dimensional, CFD-based erosion prediction procedure* (Doctoral dissertation, University of Tulsa).

Finnie, I. (1960). Erosion of surfaces by solid particles. *Wear* 3(2), 87-103.

Gnanavelu, A., N. Kapur, A. Neville and J. F. Flores (2009). An integrated methodology for predicting material wear rates due to erosion. *Wear* 267(11), 1935-1944.

Gnanavelu, A., N. Kapur, A. Neville and J. F. Flores (2009). An integrated methodology for predicting material wear rates due to erosion. *Wear* 267(11), 1935-1944.

Grant, G. and W. Tabakoff (1973). An experimental investigation of the erosive characteristics of 2024 aluminum alloy (No. 73-37). CINCINNATI UNIVERSITY OH DEPT OF AEROSPACE ENGINEERING.

Grant, G. and W. Tabakoff (1975). Erosion

prediction in turbomachinery resulting from environmental solid particles. *Journal of Aircraft* 12(5), 471-478.

Huang, C., P. Minev, J. Luo and K. Nandakumar (2010). A phenomenological model for erosion of material in a horizontal slurry pipeline flow. *Wear* 269(3-4), 190-196.

Huang, C., S. Chiovelli, P. Minev, J. Luo and K. Nandakumar (2008). A comprehensive phenomenological model for erosion of materials in jet flow. *Powder Technology* 187(3), 273-279.

Mansouri, A., H. Arabnejad, S. Karimi, S. A. Shirazi and B. S. McLaury (2015). Improved CFD modeling and validation of erosion damage due to fine sand particles. *Wear* 338, 339-350.

Mansouri, A., S. A. Shirazi and B. S. McLaury (2014). Experimental and numerical investigation of the effect of viscosity and particle size on the erosion damage caused by solid particles. In ASME 2014 4th Joint US-European Fluids Engineering Division Summer Meeting collocated with the *ASME 2014 12th International Conference on Nanochannels, Microchannels, and Minichannels* (pp. V01DT31A002-V01DT31A002). American Society of Mechanical Engineers.

Mazumder, Q. H. (2012). Effect of liquid and gas velocities on magnitude and location of maximum erosion in U-bend. *Open Journal of Fluid Dynamics* 2(2), 29.

McLaury, B. S., X. Chen and S. A. Shirazi (2004). Application and experimental validation of a computational fluid dynamics (CFD)-based erosion prediction model in elbows and plugged tees. Computers & Fluids, 33(10), 1251-1272.

Modi, O. P., R. Dasgupta, B. K. Prasad, A. K. Jha, A. H. Yegneswaran and G. Dixit (2000). Erosion of a high-carbon steel in coal and bottom-ash slurries. *Journal of materials engineering and performance* 9(5), 522-529.

Neilson, J. H. and A. Gilchrist (1968) Erosion by a stream of solid particles, *Wear*, 11 111 - 122.

Oka, Y. I., K. Okamura and T. Yoshida (2005). Practical estimation of erosion damage caused by solid particle impact: Part 1: Effects of impact parameters on a predictive equation. *Wear* 259(1-6), 95-101.

Oka, Y. I., K. Okamura and T. Yoshida (2005). Practical estimation of erosion damage caused by solid particle impact: Part 1: Effects of impact parameters on a predictive equation. Wear, 259(1-6), 95-101.

Okita, R., Y. Zhang, B. S. McLaury and S. A. Shirazi (2012). Experimental and computational investigations to evaluate the effects of fluid viscosity and particle size on erosion damage. *Journal of Fluids Engineering* 134(6), 061301.

Sadrizadeh, S., A. Nejad Ghafar, A. Halilovic and U. Hakansson (2017). Numerical, Experimental and Analytical Studies on Fluid Flow through a Marsh Funnel. *Journal of Applied Fluid Mechanics 10*(6), 1501-1507.

Safaei, M. R., O. Mahian, F. Garoosi, K. Hooman, A. Karimipour, S. N. Kazi and S. Gharehkhani (2014). Investigation of micro-and nanosized particle erosion in a 90 pipe bend using a two-phase discrete phase model. *The scientific world journal* 12.

Shehadeh, M. and A. El-Shenawy (2014). Prognosis the Erosion-Corrosion Rates for Slurry Seawater Flow in Steel Pipeline Using Neural System. Advanced Materials Research.

Shimizu, K., T. Noguchi, H. Seitoh, M. Okadab and Y. Matsubara (2001). FEM analysis of erosive wear, *Wear* 250, 779–784.

Shirani, E. and F. Ghadiri (2011). Modeling and Simulation of Interfacial Turbulent Flows. *Journal of Applied Fluid Mechanics* 4(2).

Shyji, S., M. Deepu, N. A. Kumar and T. Jayachandran (2017). Numerical Studies on Thrust Augmentation in High Area Ratio Rocket Nozzles by Secondary Injection. *Journal of Applied Fluid Mechanics*, 10(6).

Singh, J. P., S. Kumar and S. K. Mohapatra (2017). Modelling of two phase solid-liquid flow in horizontal pipe using computational fluid dynamics technique. *International Journal of Hydrogen Energy* 42(31), 20133-20137.

Singh, J., S. Kumar, J. P. Singh, P. Kumar and S. K. Mohapatra (2018). CFD modeling of erosion wear in pipe bend for the flow of bottom ash suspension. *Particulate Science and Technology* 1-11.

Solnordal, C. B., C. Y. Wong and J. Boulanger (2015). An experimental and numerical analysis of erosion caused by sand pneumatically conveyed through a standard pipe elbow. *Wear* 336, 43-57.

Talbi, K., Z. Nemouchi, A. Donnot and N. Belghar (2011). An experimental study and a numerical simulation of the turbulent flow under the vortex finder of a cyclone separator. *Journal of Applied Fluid Mechanics 4*(1), 69-75.

Wang, J. and S. A. Shirazi (2003). A CFD based correlation for erosion factor for long-radius elbows and bends. *Journal of energy resources technology* 125(1), 26-34.

Wang, W., B. Lu and J. Li, (2009). Searching for a mesh-independent sub-grid model for CFD simulation of gas–solid riser flows. *Chemical Engineering Science* 64(15), 3437-3447.

Wood, R. J. K., T. F. Jones, J. Ganeshalingam and N. J. Miles (2004). Comparison of predicted and experimental erosion estimates in slurry ducts. *Wear* 256(9-10), 937-947.

Wood, R. J. K., T. F. Jones, J. Ganeshalingam and N. J. Miles (2004). Comparison of predicted and experimental erosion estimates in slurry ducts. *Wear* 256(9-10), 937-947.

Zeng, L., G. A. Zhang and X. P. Guo (2014). Erosion–corrosion at different locations of X65 carbon steel elbow. *Corrosion Science* 85, 318-330.

Zhang, H., Y. Tan, D. Yang, F. X. Trias, S. Jiang, Y. Sheng and A. Oliva (2012). Numerical investigation of the location of maximum erosive wear damage in elbow: Effect of slurry velocity, bend orientation and angle of elbow. *Powder Technology* 217, 467-476.

Zhang, H., Y. Tan, D. Yang, F. X. Trias, S. Jiang, Y. Sheng and A. Oliva (2012). Numerical investigation of the location of maximum erosive wear damage in elbow: Effect of slurry velocity, bend orientation and angle of elbow. *Powder Technology*, 217, 467-476.

Zhang, Y., E.P. Reuterfors, B.S. McLaury, S.A. Shirazi and E.F. Rybicki (2007). Comparison of computed and measured particle velocities and erosion in water and air flows. *Wear* 263 (1) 330–338.